2023 IEEE/RSJ International Conference on Intelligent Robots and Systems (IROS)
October 1-5, 2023. Detroit, USA

Harnessing the Power of Human Biomechanics in Force-Position Domain: A 3D Passivity Index Map for Upper Limb Physical Human-(Tele)Robot Interaction

Xingyuan Zhou*, *Student Member, IEEE,* Peter Paik*, *Student Member, IEEE,*
S. Farokh Atashzar†, *Senior Member, IEEE*

2023 IEEE/RSJ International Conference on Intelligent Robots and Systems (IROS) | 978-1-6654-9190-7/23/$31.00 ©2023 IEEE | DOI: 10.1109/IROS55552.2023.10341393

***Abstract*— In the context of physical human-(tele)robot interaction, passivity-based stabilizers have been used to guarantee the physical or (tele)physical stability. In most of these examples, human biomechanics is considered an inherently passive system that dissipates energy. This assumption may not hold true when the interaction is implemented in the force-position domain, even though such a setting would be needed to boost positional accuracy and avoid the common kinematic drifts in the force-velocity domains. The aforementioned topic is examined in this paper using the concept of shortage versus excess of passivity index for human biomechanics in the force-position domain. We also investigate the compounding effect of the frequency of interaction. The outcomes of this paper will be imperative for the design of force-position domain pHRI stabilizers when the classical assumption of passivity of human biomechanics can lead to serious safety issues. In this work, for the first time, we quantitatively present the passivity margin and, thus, the energetic behavior of the human arm's biomechanics under various interaction scenarios in the Force-Position domain. The outcome of this work includes a three-dimensional passivity index map (3DPiM) that is validated on five healthy participants. The goal is to illustrate the passivity margin of the human upper limb biomechanics for two distinct levels of muscle co-contractions, as indicated by the Electromyography (EMG) signal, across four interaction frequencies and eight geometric directions. This outcome enables the future development of biomechanics-aware stabilizers in the force-position domain, quantifying the passivity margin in real-time and thus significantly reducing the stabilizer's conservatism while ensuring the safety of human-robot interactions.**

I. Introduction

In the last decade, topics related to haptics-enabled extended reality and tele-physical presence under human-centered robotics (HcR) have undergone rapid development, especially with the arrival of the next generation ultra-fast and reliable mobile communication, besides artificial intelligence and dexterous robotics [1]–[3]. By facilitating the transmission of haptic sensations from remote/virtual environments, users are provided with an intuitive and bidirectional interface that improves their overall experience and enhances the performance in remote/cloud-based tasks [4]. Thus, haptics-enabled extended reality systems can change the future of our smart and connected society when remote and tele-physical interaction can be realized with virtual renderings of real and augmented physics. In general, for haptics-enabled HcR, two crucial criteria must always be considered: (a) the overall interconnection between human biomechanics and the powerful robotic system (i.e., the haptic display) must remain stable; (b) the fidelity of the energy exchange and haptics rendering during the interaction must be maximized. However, obtaining high fidelity can often challenge stability for HcR.

Besides traditional issues such as sensor reading errors or actuator failures [5], or communication delays/jitters/packet-losses, any physical rendering that injects energy into the system (which can come from an active virtual/augmented interaction) can pose a challenge to system stability as they inject nonpassive energy into the interconnected systems [6].

Therefore, numerous approaches have been proposed to address this stability issues [7]–[11]. One state-of-the-art method is the Time Domain Passivity Approach (TDPA) [8], which ensures system stability by adaptively injecting damping into the system to guarantee a positive overall energy level, thereby enforcing passivity. Most passivity-based stabilizers, including TDPA, assume the passivity of human biomechanics, and there have been experiments supporting this concept, all in the force-velocity domain. However, the passivity of the system can be changed and challenged when the input or output of the system is redefined.

It should be noted that even though stabilizing the systems in force-velocity domains has been extensively studied in the literature, there is always concern regarding the kinematics error and position drifts due to the modification of velocity profile by the classic stabilizers for imposing the passivity. Even though there are variations of TDPA designed for reducing position drift [6], [12], this phenomenon would be inevitable and can challenge several applications that require high positional accuracy (such as surgery). To address this issue, the next generation of stabilizers can be implemented directly in the force-position domain (without any need for integration over velocity tracking errors). Even though

Xingyuan Zhou and Peter Paik are with the Department of Electrical and Computer Engineering, New York University (NYU), New York, NY, 11201 USA. Atashzar is with the Department of Electrical and Computer Engineering, Mechanical and Aerospace Engineering, and Biomedical Engineering at NYU. Atashzar is also with NYU WIRELESS Center and NYU CUSP. This material is based upon work supported by the U.S. National Science Foundation under grants #2121391 and #2208189. The work is also partially supported by NYUAD Center for Artificial Intelligence and Robotics (CAIR) award # CG010. The work is also supported in part by GAANN Grant Number P200A210062.

* Xingyuan and Peter Paik contributed equally to this work and share the first authorship.

† Corresponding author: Atashzar (f.atashzar@nyu.edu).

there are efforts in this regard, there is an issue in most of the relevant literature, i.e., human biomechanics cannot be considered passive in the force-position domain. This claim is indeed intuitive since it can be mathematically shown that even the passivity of a simple linear mass-spring-damper system (which is a dissipative system in the force-velocity domain) can be challenged at higher frequencies in the force-position domain. In other words, while it is typically acceptable and intuitive to assume that the human arm is passive in the force-velocity domain, it has been demonstrated that it can become nonpassive in the force-position domain [13], posing a challenge to the stability of the system when implementing the stabilizer built under this assumption.

In this work, for the first time, we quantitatively evaluate the passivity index (i.e., energetic behavior) of the human arm's biomechanics when encountering various interaction scenarios in the force-position domain. The outcome of this paper is presented as a three-dimensional passivity index map (3DPiM), which demonstrates the passivity margin/index of the human upper limb biomechanics for two distinct levels of muscle co-contractions, as indicated by the Electromyography (EMG) signal across four interaction frequencies and eight geometric directions.

To generate the biomechanical passivity index map, we conducted a series of systematic experiments with five healthy subjects. Our results show that the combination of interaction direction, frequency, and muscle co-contraction significantly affects the passivity level of human biomechanics in the force-position domain. This outcome enables the future development of biomechanics-aware stabilizers in the force-position domain, quantifying the passivity margin in real time and thus significantly reducing the stabilizer's conservatism while ensuring the safety of human-robot interactions. The rest of this paper is structured as follows. Section II provides the preliminary foundation of the paper. In Section III, we present the experimental methodology, and the results and discussion about the proposed 3DPiM are shown in Section IV. We concluded the paper in Section V .

II. Preliminaries

To gain a deeper comprehension of the performance of the human upper limb's biomechanics, it is common to assume that the dynamics of the limb can be represented by a linear second-order mass-spring-damper system model [14]–[17]. The linearity assumption is relaxed later in this paper. This model (given here as an example) can be denoted as:

$$M\ddot{x}(t) + B\dot{x}(t) + Kx(t) = f(t), \tag{1}$$

where $x(t)$ is the displacement of the human hand and $f(t)$ is the applied force on the hand. M, B, and K are all positive semi-definite matrices that relate to the limb's inertial, damping, and stiffness coefficients. This model can provide a basic understanding of the human upper limb regarding the corresponding energetic behavior, which is later expanded in this paper. The linear model expressed in (1) can be analyzed for passivity in both the force-velocity domain, where the velocity is the output, and the force-position domain, where the position is the output.

Force-Velocity Domain: The human upper limb's biomechanics has been extensively studied in the force-velocity domain by the authors and others and has been proven to be passive using positive realness of the corresponding transfer function (details on the related conditions can be found in [13], [18]–[21]). Deriving the admittance model of the human limb from (1) in the Laplace domain, we have:

$$H(s) = \frac{V(s)}{F(s)} = \frac{1}{(Ms + B + K/s)} \tag{2}$$

Since $H(j\omega) + H(-j\omega) \geq 0$ holds for $\forall\omega$, the linear representation of the human upper limb is categorized as positively real and thus passive [22] in the force-velocity domain. Therefore, the human upper limb is considered a passive system in the force-velocity domain interactions.

Force-Position Domain: In the force-position domain, the linear classic model of the human limb is given as

$$H(s) = \frac{X(s)}{F(s)} = \frac{1}{(Ms^2 + Bs + K)} \tag{3}$$

In this case, however, it can be found that the condition $H(j\omega) + H(-j\omega) \geq 0$ is not fulfilled when $\omega \geq \sqrt{K/M}$ (see [13] for more details). Consequently, the positive realness, and thus the passivity of the human upper limb, is not always guaranteed in the force-position domain. This can be seen by the fact that the passivity relies on the interactional frequency. In the rest of this paper, we will discuss the passivity of human biomechanics without the need for the assumption on linearity. Some definitions based on input-output relationship are given below.

Definition 1 (System's Passivity): Relaxing the assumption of linearity and without relying on the transfer function of the system (even if available), a system is passive if we have

$$\int_0^\infty U(t)^T Y(t) dt \geq -\beta, \tag{4}$$

where the input vector is denoted by $U(t)$ and the output vector is denoted by $Y(t)$. Also β is the initial energy which is often considered zero in robotics. The system's passivity is an input-output condition that examines the energy flow into a system. If the net energy is positive, the system is considered passive (i.e., dissipates energy).

Capitalizing on the definition above and to quantify the mathematical margin of passivity of the human upper limb biomechanics, the output strictly passive (OSP) condition is investigated through a series of experiments in this paper as given below.

Definition 2 (Output Strictly Passive System): A system is output strictly passive if we have

$$\int_0^\infty U(t)^T Y(t) dt \geq \xi \int_0^\infty Y(t)^T Y(t) dt - \beta. \tag{5}$$

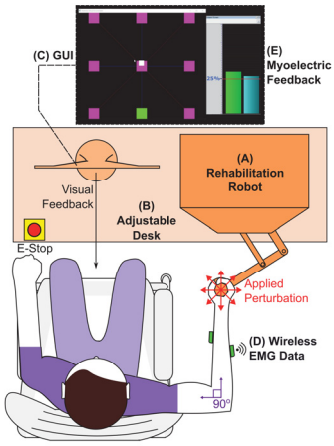

Fig. 1. Experimental set-up showing: (A) Quanser Rehabilitation Robot, (B) height-adjustable table, (C) User Interface, (D) Delsys Sensors, and (E) Electromyographic Bar Feedback.

Where ξ is the passivity index, a mathematical margin that represents the quantifiable extent of passivity which can be also considered for human biomechanics. When $\xi > 0$, we consider the human upper limb as an output strictly passive system that can absorb additional energy; thus, in this case, ξ is called the Excess of Passivity (EoP). Also, when $\xi < 0$, the human upper limb is considered an output nonpassive system that acts as an energy-generating element, and ξ is considered the Shortage of Passivity (SoP).

III. Methodology

A. Experimental Set-up

An offline identification experiment was conducted to evaluate the human upper limb's passivity margin. The experimental apparatus and corresponding experimental set-up are depicted in Fig. 1. During the identification process, the subjects were instructed to grasp the robot handle firmly, ensuring that all fingers and the palm were attached to the handle surface. Then the robot starts perturbing the subject's limb under different preset conditions, including two muscle co-contractions levels, eight directions, and four perturbation frequencies. This enabled a thorough evaluation of the passivity margin of the human limb biomechanics in various interaction scenarios. Throughout the perturbation, all the necessary force, and corresponding motion are recorded for analysis.

To ensure consistency, a standardized protocol and apparatus were developed and utilized (as depicted in Fig. 1). The experimental set-up comprised of the following components: 1) A robotic system that delivered perturbations, 2) An EMG system that measured muscle co-contraction level, 3) A visual myo-feedback guidance GUI that supplied the user with real-time information on the level of muscle co-contraction during data collection, and 4) A height-adjustable table to regulate the user's posture during the experiment.

Specifically, we utilized a 2 Degree of Freedom (DoF) rehabilitation robot (Quanser, Markham, ON, Canada) to perturb the subject's upper limb. This device provides powerful force in the X-Y plane and record force, velocity, and motion information concurrently. For measuring the EMG signal, we used a sixteen-channel wireless Bipolar Delsys Trigno system (Delsys, Natick, MA, USA). We placed bipolar EMG electrodes on the subject's skin over the muscles of interest, which enabled us to measure real-time muscle activation data during physical movements. In this study, we attached EMG electrodes to the subject's dominant forearm, placing four electrodes along each of the muscles: extensor digitorum, extensor carpi ulnaris, brachioradialis, and flexor carpi radialis to capture muscle activity while grasping the robot handle.

Furthermore, we used real-time EMG data to provide visual myo-feedback to indicate the muscle co-contraction level. At the same time, the user performed the task prescribed by the protocol (explained later). To regulate the subject's posture during the identification process, we used a height-adjustable table, which ensured that the subject's upper arm and forearm were perpendicular when reaching the central position. This posture was maintained consistently for all subjects throughout the experiment.

During the experiment, the subjects were provided with graphical visual feedback consisting of two components. The first component was the user interface, which demonstrated the robot's end-effector motion and the perturbation's direction. The white dot in the GUI indicated the current position of the end-effector, while the purple/green dots indicated the desired/current perturbation directions. The second component was the myo-feedback, which was presented in a bar form and represented the percentage of maximum voluntary contraction (%MVC) of two selective sensors that were the most sensitive sensors through our observation in this experiment. Throughout the experiment, subjects were instructed to hold the handle at the prescribed muscle coactivation illustrated by the real-time myo-feedback bar while minimizing any voluntary motion to the handle in response to the robot's perturbations.

B. Experimental Procedure

The overall experiment can be categorized into two stages: 1) estimate the MVC, which was then used for real-time muscle-contraction myo-feedback 2) conduct the identification process in random order (including two muscle co-contraction conditions, four perturbation frequencies, and eight geometric perturbation directions).

In the first stage, the subjects were instructed to grasp the robot handle as hard as possible for three seconds, followed by the same amount of time for resting and repeating the same process. Therefore, the MVC of the subjects is acquired and used for myo-feedback guidance. The myo-feedback was provided in the format of a percentage of MVC, which was calculated based on the RMS value of the real-time EMG data recording, normalized to their corresponding recorded MVC values.

In the second stage, we considered four different perturbation frequencies to test: 0.5Hz, 1Hz, 1.5Hz, and 2Hz, which are the representative frequency ranges of most activities of daily living. Besides, we also investigated the result in

TABLE I
DEMOGRAPHIC DATA

Subject	Height (m)	Weight (kg)	Age	Sex
1	1.62	58	24	M
2	1.70	57	24	F
3	1.77	64	25	M
4	1.73	62	33	F
5	1.80	75	23	M

two grasp conditions: relax condition, where the subjects are asked to hold the robot handle with minimal voluntary muscle activation. Stiff condition, where the subjects are instructed to maintain 25%MVC through each perturbation period. The perturbation movement of the robot handle follows a sinusoidal oscillation at the preset frequencies in one of the eight different geometric directions, as shown in the GUI.

C. Participants

The study involved five healthy participants, comprising three males and two females, with ages ranging from 27 ± 5. The institutional review board of New York University approved the study, and all subjects were provided with a comprehensive study description and gave written consent. None of the participants reported a history of diagnosed/known neurological injury. All the subjects are right-hand dominant. Detailed demographic information is provided in Table I.

D. Data Analysis and EoP Calculation

By applying the OSP condition derived from the nonlinear control theory, we can assess the passivity margin of the human biomechanics during the interaction. In this regard, a perturbation force 'f' is applied to the human's arm, resulting in the relevant position 'p' of the arm during the interaction. The passivity margin (i.e. EoP) under the muscle activation level 'm', interaction frequency 'ω', and geometric direction 'i', can be expressed as follows:

$$\xi_{m,\omega,i} = \frac{\int_{T_s}^{T_e} f_{m,\omega,i}(t)^T p_{m,\omega,i}(t) dt}{\int_{T_s}^{T_e} p_{m,\omega,i}(t)^T p_{m,\omega,i}(t) dt}, \tag{6}$$

In (6), ξ is the resulting passivity margin of the limb during the interaction. T_s and T_e represented the start and end times of the last five-second calculation window for each perturbation direction to avoid the artifacts related to directional changes. The perturbation time at each direction was around 10 seconds. A positive value of ξ represents the EoP of the human biomechanics, and the higher value of the ξ represents that human biomechanics has stronger energy absorption capability during pHRI in force-position domain. Conversely, a negative value of ξ represents SoP, indicating the energy-generating capability during pHRI in force-position domain. The more negative the ξ, the greater stability challenges it would pose when connected to the network teleoperation system.

IV. RESULTS

The three-dimensional passivity index maps (3DPiMs) of each subject for relaxed muscle co-contraction are shown in Fig. 2. Likewise, the 3DPiMs of each subject for the stiff muscle co-contraction are shown in Fig. 3. The 3DPiMs shows the corresponding ξ value given a perturbation direction and perturbation frequency. The eight perturbation directions are indicated on the 3DPiMs of subject 1, showing the directions labelled from $0°$ to $315°$. The perturbation frequencies increase as they go further from the origin, and their levels are related by squares shown on the 3DPiM. The ξ values are color-coded according to a set color bar range. For the relaxed 3DPiMs, the range is from -100 to 100 Ns/m. For the stiff 3DPiMs, the range is from -200 to 200 Ns/m. In addition, the 3DPiMs are shown in two-dimensions using these color values next to the 3DPiMs.

Based on a visual inspection, the ξ values generally decrease as the frequency increases. This phenomenon can be observed for each subject, direction, and relaxed and stiff muscle co-contractions. This is expected based on the definition of positive realness in the force-position domain derived in Section II, where the passivity of the system is lost when $\omega \geq \sqrt{K/M}$.

V. DISCUSSION

Besides the visual inspection, in order to have a better understanding of how the ξ values change under different frequency groups and frequencies, violin plots with statistical test results are provided as follows.

In Fig. 4(a), changes in the ξ values between frequency groups are investigated for the relaxed muscle co-contraction. The ξ values of all subjects are combined and separated into four frequency groups: 0.5 Hz, 1 Hz, 1.5 Hz, and 2 Hz. Their violin plot distributions are shown in Fig. 4(a). Through the Kolmogorov-Smirnov normality test, the distributions were found to be non-normal [23]. Therefore, Wilcoxon signed-rank test was used to evaluate the statistical significance between distributions with a threshold of $p < 0.05$ [24]. The results show that there is no significant difference in the ξ values between 0.5 Hz and 1 Hz. However, there is a significant decrease in the ξ values when the frequency increases beyond 1 Hz. This follows the observed trend in the 3DPiMs, where the ξ values increase in some directions between 0.5 Hz and 1 Hz but decrease beyond 1 Hz. This is also verified by condition of positive realness described above, where the human dynamics can still be passive below a certain frequency. Thus, this threshold may exist between 1 and 1.5 Hz in certain directions during relaxed muscle co-contraction levels.

In Fig. 4(b), changes in the ξ values between frequency groups are investigated for the stiff muscle co-contraction. The data is distributed into four groups in the same way. Again, the distributions were found to be non-normal, and the Wilcoxon signed-rank test was used. The same observances can be made between frequency groups for stiff muscle co-contractions. However, the ξ values appear to vary more

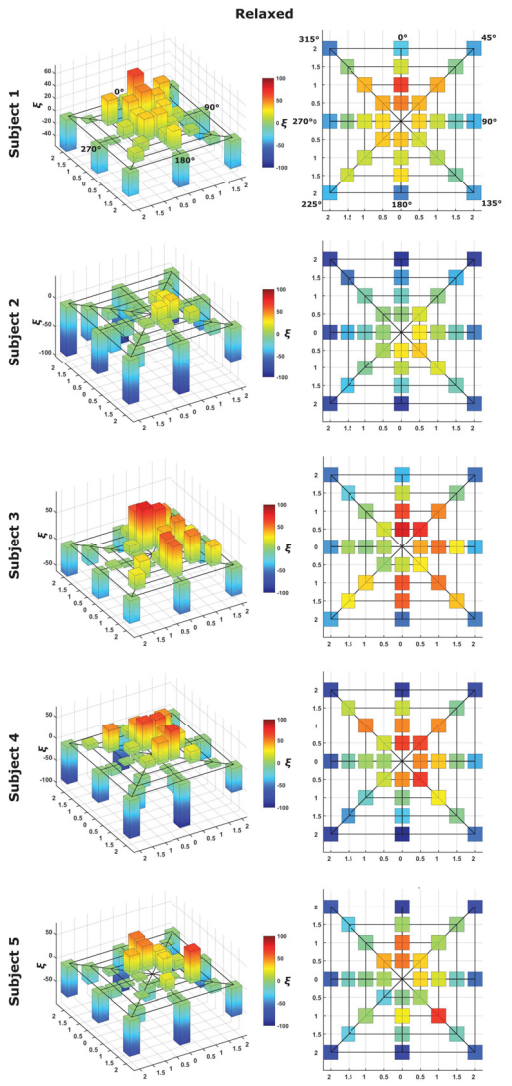

Fig. 2. Resulting Three-Dimensional Passivity Index Maps for each subject during a relaxed muscle co-contraction. The two-dimensional map equivalent is shown to the right of the 3DPiM. The ξ color bar values range from -100 to 100 Ns/m.

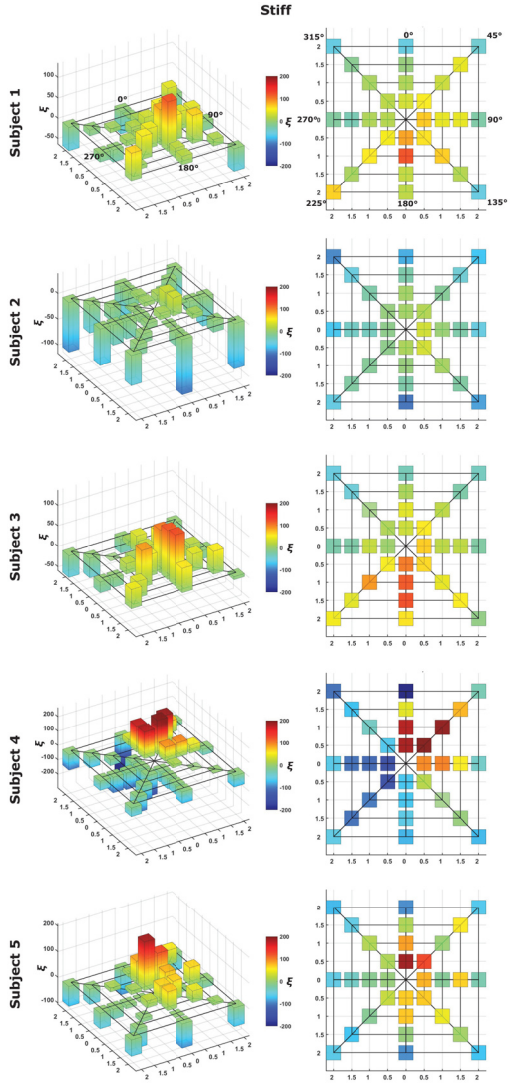

Fig. 3. Resulting Three-Dimensional Passivity Index Maps for each subject during a stiff muscle co-contraction. The two-dimensional map equivalent is shown to the right of the 3DPiM. The ξ color bar values range from -200 to 200 Ns/m.

for stiff muscle co-contraction than for relaxed muscle co-contractions.

To analyze the trend of how the passivity index decreases as the frequency increases, a plot of the mean ξ at each frequency for all directions is created and shown in Fig. 5.

In Fig. 5(a), the change in the ξ values between different directions as the frequency increases are visualized for the relaxed muscle co-contraction. In this regard, we take the ξ values between all 5 subjects for each perturbation direction and frequency and calculate the mean (32 resulting mean ξ values; 4 ξ values in each direction where each value pertains to the mean ξ value of a given frequency). A line is plotted for each direction where the y-axis represents the mean ξ value and the x-axis represents the frequency. The mean and standard deviation of all eight directions are plotted as a black line and shaded region respectively. As can be seen, the ξ values decrease in all eight directions. In addition, the standard deviation decreases as the frequency increases. This result shows there is less variance in the ξ values between subjects as the frequency of interaction increases.

The corresponding plot for the stiff muscle co-contraction is presented in Fig. 5(b). A similar trend is observed where the ξ values decrease as the frequency increases. However, this trend is broken in some directions (225° and 270°). This may indicate that there is a change in the overall dynamics of the human limb in those directions. Unsurprisingly, these are the directions when the robot handle is perturbating in the direction of the human torso.In addition, compared to the standard deviation seen in the relaxed slopes, the standard deviation is larger for the stiff slopes. This shows that there is a larger variance in the ξ values between subjects during stiff muscle co-contraction than during to relaxed muscle co-contraction. This validates the observances seen in both the 3DPiMs and the violin plots.

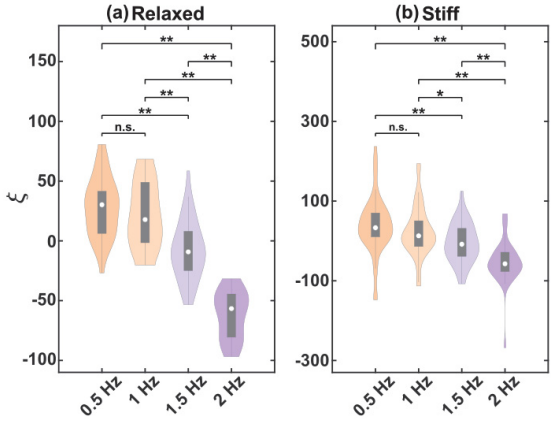

Fig. 4. Violin Plots comparing ξ values between different frequency groups for the relaxed muscle co-contraction (a) and stiff muscle co-contraction (b). For a given frequency group, the ξ value of all 5 subject in all 8 directions are combined to form one distribution ($n = 40$). Between all groups, except the 0.5Hz and 1Hz groups, there was a statistical significance (*Wilcoxon Signed-rank:* $p < 0.001$ *('**') and* $p < 0.05$ *('*')*).

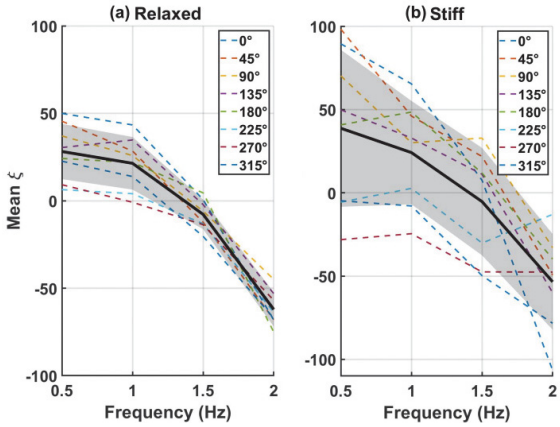

Fig. 5. Plot showing mean ξ value progression as the frequency increases in each direction for relaxed muscle co-contraction (a) and stiff muscle co-contraction (b). The mean and standard deviation of all the directions are shown as a solid black line and shaded region.

VI. Conclusion

In this paper, a three-dimensional passivity index map (3DPiMs) was introduced, which quantitatively illustrated the energetic behavior of the human upper limb during Force-Position domain interactions while considering the interaction frequencies, geometric directions, and muscle activity level. The 3DPiM design relaxes the classic assumption of the linearity and passivity of human biomechanics and can be directly used to develop a biomechanics-aware passivity-based stabilizer in the Force-Position with the goal of maximizing the utilization of the encoded energetic capacity of human biomechanics to reduce the conservatism of the stabilizers and enhance the fidelity of force rendering. The study involved five participants, and the results demonstrated that the passivity margin of the human biomechanics in the force-position domain is a compound factor influenced by the interactional frequencies, geometric directionality, and muscle co-contraction activity level. Specifically, as the interactional frequencies increase, there is a clear trend that the passivity margin transitions from positive to negative, and the transition frequencies vary among subjects. The statistical evaluation was performed using the Wilcoxon signed-rank test.

References

[1] L. Onnasch and E. Roesler, "A taxonomy to structure and analyze human–robot interaction," *International Journal of Social Robotics*, vol. 13, no. 4, pp. 833–849, 2021.

[2] A. Mohebbi, "Human-robot interaction in rehabilitation and assistance: a review," *Current Robotics Reports*, vol. 1, pp. 131–144, 2020.

[3] S. Avgousti *et al.*, "Medical telerobotic systems: current status and future trends," *Biomedical engineering online*, vol. 15, no. 1, pp. 1–44, 2016.

[4] V. Villani *et al.*, "Survey on human–robot collaboration in industrial settings: Safety, intuitive interfaces and applications," *Mechatronics*, vol. 55, pp. 248–266, 2018.

[5] M. Shahbazi *et al.*, "Robotics-assisted mirror rehabilitation therapy: a therapist-in-the-loop assist-as-needed architecture," *IEEE/ASME Transactions on Mechatronics*, vol. 21, no. 4, pp. 1954–1965, 2016.

[6] V. Chawda and M. K. O'Malley, "Position synchronization in bilateral teleoperation under time-varying communication delays," *Ieee/asme transactions on mechatronics*, vol. 20, no. 1, pp. 245–253, 2014.

[7] S. F. Atashzar *et al.*, "A small-gain approach for nonpassive bilateral telerobotic rehabilitation: Stability analysis and controller synthesis," *IEEE Transactions on Robotics*, vol. 33, no. 1, pp. 49–66, 2016.

[8] J.-H. Ryu *et al.*, "Stability guaranteed control: Time domain passivity approach," *IEEE Transactions on Control Systems Technology*, vol. 12, no. 6, pp. 860–868, 2004.

[9] S. P. Buerger and N. Hogan, "Complementary stability and loop shaping for improved human–robot interaction," *IEEE Transactions on Robotics*, vol. 23, no. 2, pp. 232–244, 2007.

[10] E. Spyrakos-Papastavridis *et al.*, "Passivity preservation for variable impedance control of compliant robots," *IEEE/ASME Transactions on Mechatronics*, vol. 25, no. 5, pp. 2342–2353, 2019.

[11] B. Hannaford and J.-H. Ryu, "Time-domain passivity control of haptic interfaces," *IEEE transactions on Robotics and Automation*, vol. 18, no. 1, pp. 1–10, 2002.

[12] J. Artigas *et al.*, "Position drift compensation in time domain passivity based teleoperation," in *2010 IEEE/RSJ International Conference on Intelligent Robots and Systems*, 2010, pp. 4250–4256.

[13] M. Shahbazi *et al.*, "Position-force domain passivity of the human arm in telerobotic systems," *IEEE/ASME Transactions on Mechatronics*, vol. 23, no. 2, pp. 552–562, 2018.

[14] G. K. I. K. Tsuji T, Morasso PG, "Human hand impedance characteristics during maintained posture," *Biol Cybern.*, vol. 72, no. 6, pp. 475–485, 1995.

[15] L. Masia and V. Squeri, "A modular mechatronic device for arm stiffness estimation in human–robot interaction," *IEEE/ASME Transactions on Mechatronics*, vol. 20, no. 5, pp. 2053–2066, 2015.

[16] M. Dyck and M. Tavakoli, "Measuring the dynamic impedance of the human arm without a force sensor," in *2013 IEEE 13th International Conference on Rehabilitation Robotics (ICORR)*, 2013, pp. 1–8.

[17] P. H. McCrea *et al.*, "Linear spring-damper model of the hypertonic elbow: reliability and validity," *Journal of Neuroscience Methods*, vol. 128, no. 1, pp. 121–128, 2003.

[18] S. F. Atashzar *et al.*, "A passivity-based approach for stable patient–robot interaction in haptics-enabled rehabilitation systems: modulated time-domain passivity control," *IEEE Transactions on Control Systems Technology*, vol. 25, no. 3, pp. 991–1006, 2016.

[19] S. F. Atashzar *et al.*, "Energetic passivity decoding of human hip joint for physical human-robot interaction," *IEEE Robotics and Automation Letters*, vol. 5, no. 4, pp. 5953–5960, 2020.

[20] M. Vidyasagar, ", nonlinear systems analysis," *Philadelphia, PA, USA: SIAM*, vol. 42, no. 1, pp. 1–10, 2002.

[21] P. M. D.J. Hill, "Stability results for nonlinear feedback systems," *Automatica*, vol. 13, no. 4, pp. 377–382, 1977.

[22] M. Vidyasagar, *Nonlinear systems analysis*. SIAM, 2002.

[23] R. F. Woolson, "Wilcoxon signed-rank test," *Wiley encyclopedia of clinical trials*, pp. 1–3, 2007.

[24] H. W. Lilliefors, "On the kolmogorov-smirnov test for normality with mean and variance unknown," *Journal of the American statistical Association*, vol. 62, no. 318, pp. 399–402, 1967.